Numerical Simulations of Convection with a Horizontal Magnetic Field

by

Talal A. Al-Refae

B.A., Physics, University of Colorado Boulder

B.A., Mathematics, University of Colorado Boulder

Defense Date: 04/05/2019

Research Advisor: Michael A. Calkins (Physics)

Honors Council Representative: John Cumalat (Physics)

Committee Member: Mark Rast (Astrophysics)

A thesis submitted to the faculty of the

University of Colorado in partial fulfillment

of the requirements for the award of

departmental honors in the

Department of Physics

2019

This thesis entitled:
Numerical Simulations of Convection with a Horizontal Magnetic Field
written by Talal A. Al-Refae
has been approved for the Department of Physics

_____

Prof. Michael A. Calkins

_____

Prof. John Cumalat

_____

Prof. Mark Rast

Date _____

The final copy of this thesis has been examined by the signatories, and we find that both the content and the form meet acceptable presentation standards of scholarly work in the above mentioned discipline.

Al-Refae, Talal A. (B.A., Physics)

Numerical Simulations of Convection with a Horizontal Magnetic Field

Thesis directed by Prof. Michael A. Calkins

A numerical study of magnetoconvection with a horizontal magnetic field in a plane layer geometry is conducted. Novel dynamical regimes are observed beyond those occurring in classical (i.e non-magnetic) Rayleigh-Bénard convection. Imposed magnetic field strengths up to Chandrasekhar numbers of $Q = 10^6$ are investigated. The most unstable flow configuration is two-dimensional rolls oriented parallel to the direction of the imposed magnetic field in which the induced magnetic field is identically zero. The convective roll structure exhibits a preferential flow alignment along the direction of the imposed magnetic field thereby sustaining an anisotropic flow field. Deviations away from the convective roll structure induce a magnetic field separate from the externally-imposed magnetic field. For weak magnetic field strengths ($Q = 10^2$), we observe the $Nu \sim Ra^{2/7}$ scaling law, where Nu is the Nusselt number, though the overall heat transfer is less than that observed in non-magnetic Rayleigh-Bénard convection; we hypothesize this reduction is due to the presence of ohmic dissipation. For $Q = 10^4$ and 10^6 we find that the two-dimensional convective roll structure is maintained for Ra values orders of magnitude larger than the critical Rayleigh number. In this flow regime our calculations suggest a $Nu \sim Ra^{0.37}$ power law. Two-dimensional turbulence is not observed in any of the imposed magnetic field regimes, rather we observe turbulent flow behavior when the flow becomes three-dimensional. For $Q = 10^4$ we observe the development of large-scale modulations along the direction of the magnetic field when $Ra \geq 6 \times 10^5$. For $Q = 10^4$ and $6 \times 10^5 \leq Ra \leq 10^7$ the $Nu \sim Ra^{2/7}$ power law is observed.

In general, for sufficiently strong magnetic fields, we find three primary regimes: (1) laminar, 2D convection with a heat transfer scaling that exceeds $Nu \sim Ra^{1/3}$; (2) a transitional region where 3D modulations begin and the heat transfer scaling law is reduced; and (3) anisotropic 3D convection with $Nu \sim Ra^{2/7}$ but with an overall heat transfer that is always less than the hydrodynamic case.

A fourth regime at very high Rayleigh numbers, in which the convection is no longer influenced by the magnetic field, is hypothesized to occur, but not observed in the simulations.

Dedication

To my parents and brothers.

Acknowledgements

Many thanks must first be given to my research advisor Professor Michael Andrew Calkins for his unending source of support, humor, and guidance. I am indebted to Mike for his exciting and enlightening introduction to the life of a researcher. My upmost respect and gratitude must also be sent to Dr. Stefano Maffei for his inhuman patience and meticulous attention for detail, both of which have benefited me greatly. I further thank Ming Yan for introducing me to the simulation code and for providing me with some of his initial simulation data for reference.

My love is sent to my family for their indispensable support and encouragement in all my endeavors.

Contents

Tables

Table

Figures

Figure

Chapter 1

Introduction

Thermal convection plays an integral dynamical role in a wide variety of physical phenomena and industrial applications. Continental drifts as well as many other fundamental tectonic processes are largely believed to be caused by convective heat transfer in the Earth's crust [2]. Buoyancy driven convective flow is a primary source of fluid motion within the interior of celestial bodies [3]. Magnetically influenced convection has been a topic of great interest for its applicability to the surface and interior of stars such as the Sun where it is believed that electromagnetic forces significantly influence heat transfer. Observations [8] suggest that a sudden outburst of magnetic field lines from the interior of the Sun force dark pigmentations on the surface of the sun called "sunspots," as shown in Figure (1.1). The twisting flow field near the sunspot is thought to be due to convectional effects from the surrounding magnetic field approximately parallel to the surface of the sun.

In this thesis we investigate the effects of a magnetic field on the canonical model of thermal convection of the so-called Rayleigh-Bénard geometry, where a fluid layer is contained between parallel planes that are separated by a distance L. As depicted in Figure (1.2), the bottom plate is maintained at a temperature T_1 that is greater in magnitude than the top layer's temperature T_0 as to provide a forum for convection driven flow. It is assumed that there is a constant gravitational field such that $\mathbf{g} = -g\hat{\mathbf{z}}$ (where g is the magnitude of the free-fall acceleration near the surface of the Earth).

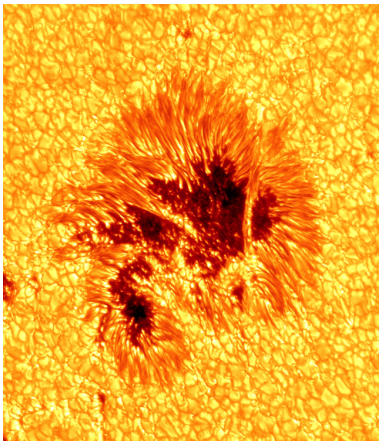

Figure 1.1: The residual flow near the dark pigmentations on the surface of the Sun are widely believed to convectional flow under the influence of a magnetic field parallel to the surface of the Sun. Image courtesy of New Jersey's Institute of Technology's Big Bear Solar Observatory.

The simple geometry of Rayleigh-Bénard convection yields interesting flow structures. The layer of fluid near the vicinity of the bottom plate expands and, due to buoyant forces, rises. When the fluid parcel is sufficiently near the top layer it is cooled and falls due its contraction. We refer to this continuous flow cycle as "convection rolls."

The convectional implications of an applied magnetic field on Rayleigh-Bénard convection is an area of open experimental and numerical research [1]. In this thesis we investigate how a magnetic field imposed in the horizontal direction (namely, in the direction perpendicular to the vertical plane in which the convection rolls occur) affects overall heat transfer and flow dynamics. We utilize direct numerical simulations to achieve an approximate solution to the governing equations. Varying magnetic field strengths are discussed in a modestly wide range of flow regimes.

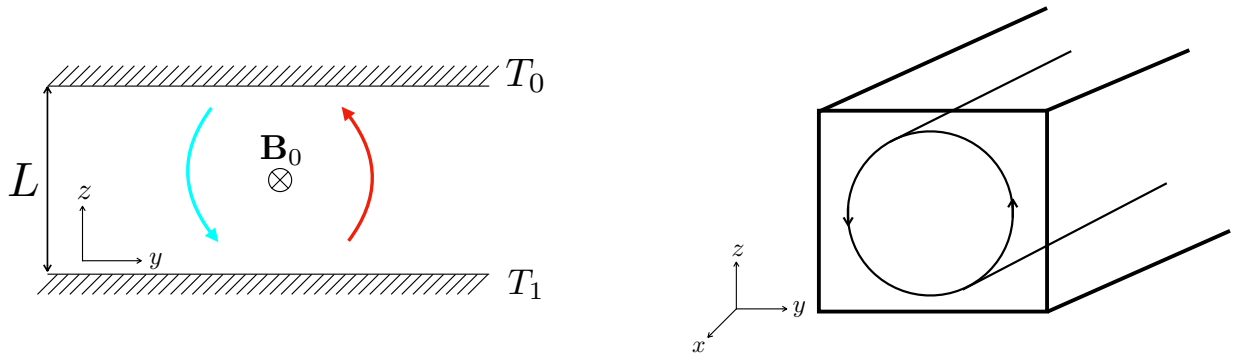

(a) (b)

Figure 1.2: The geometry of Rayleigh Bénard convection is shown. Here, two plane layers are maintained at constant temperature ($\Delta T = T_1 - T_0 > 0$). Figure (1.2a) shows the natural cycle of a fluid parcel rising due to the effects of buoyancy until it is cooled from above above and falls. We simulate the effects of an induced horizontal magnetic field ($\mathbf{B}_0$) along the x-direction. Figure (1.2b) showcases the three-dimensional roll structure observed at the onset of convection.

In Chapter 2 we briefly discuss the governing equations, relevant boundary conditions, and our nondimensionalization scheme. Further, a linear stability analysis is presented as to understand general dynamical effects of the horizontal magnetic field on the flow structure. Our simulation results are showcased in Chapter 3 where we examine trends and various flow regimes introduced by the magnetic field. Visualizations of representative flow structures will be shown as an attempt to qualitatively differentiate between flow regimes.

Chapter 2

Mathematical Background

2.1 Governing Equations

The equations governing the dynamics of fluids are statements of the conservation of mass, momentum and energy (a more complete justification of this statement of this may be found in [11] and [18]). For incompressible flow, the conservation of mass condition is derived from the continuity equation and is given by

$$\nabla \cdot \mathbf{u} = 0. \tag{2.1}$$

Our second governing equation is the the Navier-Stokes Equation

$$\rho \left(\frac{\partial}{\partial t} + \mathbf{u} \cdot \nabla \right) \mathbf{u} = -\nabla p + \mu \nabla^2 \mathbf{u} + \mathbf{F}, \tag{2.2}$$

and serves as the conservation of momentum condition for incompressible viscous fluid flow. Here, ρ is the fluid density, p denotes pressure, μ represents the viscosity of the fluid, and $\mathbf{F}$ is the collection of all external (body) forces. To incorporate the effects of convection and the magnetic field we deduce an explicit form of $\mathbf{F}$.

Non-isothermal problems are difficult to solve exactly as the behavior is often fundamentally non-linear. Moreover, a more serious difficulty arises from a thermal expansion of the fluid, thereby potentially undermining the implicit assumption of incompressibility in the preceding governing equations. If, however, the temperature variations are small, the standard so-called Bousinessq approximation may be employed to neglect higher order variations in the fluid density thereby fully preserving our first governing equation. For a Bousinessq fluid, compressibility is present only in

the buoyant force as it is the primary driving force of the flow:

$$\mathbf{F}_b = -\left(\rho_0 + \delta\rho\right)\mathbf{g} = -\nabla\left(\rho_0\Phi\right) + \delta\rho\mathbf{g}. \tag{2.3}$$

(Here, $\Phi = gz$ is a scalar potential.) The density of a Bousinessq fluid is given by

$$\rho = \rho_0\left[1 - \alpha\left(T - T_0\right)\right], \tag{2.4}$$

where α is the coefficient of cubical expansion.

The inclusion of the buoyant force into the Navier-Stokes equation yields

$$\left(\frac{\partial}{\partial t} + \mathbf{u}\cdot\nabla\right)\mathbf{u} = -\frac{1}{\rho_0}\nabla(p + \Phi) + \frac{\delta\rho}{\rho_0}\mathbf{g} + \nu\nabla^2\mathbf{u}, \tag{2.5}$$

where $\nu = \mu/\rho$ is the kinematic viscosity. It is not sensible to omit the first order correction to the gravitational force due to the fact that the local gravitational acceleration is large when compared to the flow acceleration. This causes the gravitational term to remain on the same scale as the viscosity term in the momentum equation. The Bousinessq approximation therefore states that the density variations may be neglected from the continuity and momentum equations except when $\delta\rho$ is multiplied by g.

The imposition of a magnetic field requires the addition of a Lorentz force to the momentum equation. For more detailed derivations of the hydromagnetic equations we point the reader to [5]. The Lorentz body force for a continuous charge distribution is given by

$$\mathbf{F}_L = \mathbf{J}\times\mathbf{B}. \tag{2.6}$$

So long as the flow velocity remains small when compared to the speed of light, we may neglect Maxwell's addition to Ampere's law and rewrite the Lorentz force in the following manner

$$\mathbf{F}_L = \frac{1}{\mu_0}\left(\nabla\times\mathbf{B}\right)\times\mathbf{B} = \frac{1}{\mu_0}\left[\mathbf{B}\cdot\nabla\mathbf{B} - \nabla\left(\frac{\mathbf{B}^2}{2}\right)\right], \tag{2.7}$$

where the second equality may be justified through the use of a vector identity. In addition one may utilize the curl condition of the electric field coupled with Ohm's relation $\mathbf{E} + \mathbf{v}\times\mathbf{B} = \mathbf{J}/\sigma$ to derive the induction equation

$$\frac{\partial\mathbf{B}}{\partial t} = \eta\nabla^2\mathbf{B} + \nabla\times(\mathbf{v}\times\mathbf{B}), \tag{2.8}$$

where η denotes the magnetic diffusivity of the substance.

Here, we decompose the magnetic field into an imposed field ($\mathbf{B}_0$) and an induced field ($\mathbf{b}$) such that

$$\mathbf{B} = \mathbf{B}_0 + \mathbf{b}. \tag{2.9}$$

When $\mathbf{B}_0 \gg \mathbf{b}$, we can utilize the so-called quasi-static approximation. In this limiting case, the induction equation becomes

$$\eta \nabla^2 \mathbf{B} + (\mathbf{B}_0 \cdot \nabla)\, \mathbf{u} = 0, \tag{2.10}$$

where, in this thesis, we restrict the imposed magnetic field to be a unidirectional horizontal field defined by

$$\mathbf{B}_0 = B_0 \hat{\mathbf{x}}. \tag{2.11}$$

The governing equations will further be nondimensionalized through the length, velocity, and time scales L, κ/L^2, and κ/L, respectively. As such, the list of non-dimensional governing equations is given by

$$\left(\frac{\partial}{\partial t} + \mathbf{u} \cdot \nabla\right) \mathbf{u} = -\nabla p' + \frac{\mathrm{Ra}}{\mathrm{Pr}} \theta \boldsymbol{e}_z + \mathrm{Q} \frac{\partial \mathbf{b}}{\partial x} + \mathrm{Pr}\, \nabla^2 \mathbf{u}, \tag{2.12}$$

$$\nabla^2 \mathbf{b} + \frac{\partial \mathbf{u}}{\partial x} = 0, \tag{2.13}$$

$$\left(\frac{\partial}{\partial t} + \mathbf{u} \cdot \nabla\right) \theta = \nabla^2 \theta, \tag{2.14}$$

$$\nabla \cdot \mathbf{u} = 0, \tag{2.15}$$

$$\nabla \cdot \mathbf{B} = 0, \tag{2.16}$$

where θ is the dimensionless temperature. The nondimensional parameters,

$$\mathrm{Ra} = \frac{\alpha \Delta T g L^3}{\kappa \nu}, \quad \mathrm{Pr} = \frac{\nu}{\kappa}, \quad \mathrm{Q} = \frac{B_0^2 L^2}{\rho \mu_0 \nu \eta}, \tag{2.17}$$

are the Rayleigh, thermal Prandtl, and Chandrasekar numbers, respectively. The Rayleigh number is associated with buoyancy driven flow and characterizes the ratio between the destabilizing effect of buoyancy to the stabilizing effect of viscosity. The thermal Prandtl number measures the ratio of

momentum diffusivity to thermal diffusivity and is fixed at 1 for the remainder of this thesis. The Chandrasekar number is a representation of the imposed magnetic field's strength.

For the following numerical simulations we impose impenetrable, stress-free, mechanical boundary conditions on the top and bottom electrically insulated constant temperature plates. The magnetic field is matched continuously to a harmonic potential field outside the simulation domain.

2.2 Linear Stability Analysis

A hydrodynamic stability analysis will prove to be fruitful in later discussions. A discussion of the non-magnetic case is given by Drazin [7]. We solve the magnetically constrained problem similarly using the method of normal modes. It is assumed that our system is initialized in a basic state of rest. Small sinusoidal perturbations will be introduced to the governing equations and only the first order corrections will be considered, effectively linearizing the governing equations. The linearized dimensionless momentum equation is then

$$\frac{\partial \mathbf{u}}{\partial t} = -\nabla p' + \mathrm{Ra}(\theta \mathbf{e}_z) + \mathrm{Q}\left(\frac{\partial \mathbf{b}}{\partial x}\right) + \nabla^2 \mathbf{u}. \tag{2.18}$$

The curl of the momentum equation is given by

$$\frac{\partial \omega}{\partial t} = \mathrm{Ra}\left(\nabla\theta \times \mathbf{e}_z\right) + \nabla^2\omega + \mathrm{Q}\left(\frac{\partial \mathbf{j}}{\partial x}\right), \tag{2.19}$$

where $\omega = \nabla \times \mathbf{u}$ is the vorticity of the fluid. Curling once more, the vertical component of equation (2.19) becomes

$$\frac{\partial}{\partial t}\left(\nabla^2 w\right) = \mathrm{Ra}\nabla_1^2\theta + \nabla^4 w - \mathrm{Q}\frac{\partial}{\partial x}\left(\nabla^2 b_z\right). \tag{2.20}$$

(Here, $\nabla_1^2 = \partial_{xx} + \partial_{yy}$ is the horizontal Laplacian operator.) Assuming that the onset of convection is steady, the linearized governing equations for the temperature and magnetic field allow us to rewrite equation (2.20) solely in terms of the vertical velocity

$$\nabla^6 w + \mathrm{Q}k_x^2\nabla^2 w = \mathrm{Ra}\nabla_1^2 w, \tag{2.21}$$

where k_x denotes the horizontal wavenumber in the x-direction. To obtain equation (2.21), we assumed a normal mode solution of the form

$$w = \sin(n\pi z)\exp[i(k_x x + k_y y)], \tag{2.22}$$

where k_y is the horizontal wavenumber in the y-direction. Note that equation (2.22) satisfies our mechanical boundary conditions. Solving equation (2.21), we find the general expression for the marginal stability of the Rayleigh number to be

$$\mathrm{Ra}_n(k) = \frac{\left(n^2\pi^2 + k^2\right)^3 + \mathrm{Q}k_x^2\left(n^2\pi^2 + k^2\right)}{k^2}, \tag{2.23}$$

where k is the sum of the two independent horizontal wavenumbers. We note that as $\mathrm{Q} \to 0$ we successfully restore the marginal stability relation of classical Rayleigh-Bénard convection. Evidently, the existence of a magnetic field introduces an asymmetry between the two horizontal wavenumbers that was not present in non-magnetic convection. We therefore expect the flow field to remain anisotropic as long as Q remains dynamically relevant.

Rayleigh [16] derived the theoretical requirements of convective heat transfer. The critical Rayleigh number, Ra_c, is the point in which the development of convective heat transfer is feasible. The critical Rayleigh number and wavenumber are determined by minimizing equation (2.23). We note that the magnetic term only increases Ra and hence we must force $\mathrm{Q} = 0$ in order find Ra's minimal value. This implies that the most unstable mode of the system is independent of the magnetic field. We state the critical Ra and wavenumber:

$$\mathrm{Ra}_c = \frac{27\pi^4}{4}, \quad k_c = \sqrt{\frac{\pi^2}{2}}. \tag{2.24}$$

Numerically, $\mathrm{Ra}_c \approx 658$ and $k_c \approx 2.2215$.

Chapter 3

Methods and Results

Convection in the presence of an imposed horizontal magnetic field is studied numerically in a plane layer of fluid with periodic horizontal dimensions. The vertical dimension of the governing equations is discretized using Chebyshev polynomials and the periodic horizontal dimensions are discretized with a Fourier series. We utilize a psuedo-spectral code with a third order mixed implicit explicit Runge-Kutta time-stepping scheme (RK3). For more information regarding the details of the numerical methods see Marti, Calkins and Julien (G cubed, 2016) [12] and Peyret's introduction to spectral methods for incompressible flow [14].

We consider three distinct magnetic field strengths characterized by a Chandrasekhar number Q = 10^2, 10^4, and 10^6 which, for purposes that do not extend beyond nomenclatural convenience, we shall refer to as the weak, intermediate, and strong magnetic field regimes, respectively. The magnitude of Rayleigh numbers considered range from 10^2 to 10^7 to encapsulate a wide range of flow morphologies. Our results cover the broadest range of parameters utilized in a direct numerical simulation of horizontally constrained magnetoconvection in a three-dimensional plane layer geometry to date.

The output parameters of primary interest first include the Nusselt number, defined as follows:

$$\mathrm{Nu} = \left\langle -\frac{\partial \bar{\theta}}{\partial z} \right\rangle \Big|_{z=0}, \tag{3.1}$$

where $\bar{\theta}$ denotes the horizontally and temporally averaged temperature. The Nusselt number describes the ratio of convective over conductive heat transfer and is bounded below by unity. Other

dynamical parameters of interest include the Reynolds number (Re) and the interaction parameter (N), where

$$\mathrm{Re} = \frac{UL}{\nu}, \tag{3.2}$$

and

$$\mathrm{N} = \frac{\mathrm{Q}}{\mathrm{Re}}. \tag{3.3}$$

Re describes the ratio between the inertial and viscous forces, and N signifies the dynamical relevance of the imposed magnetic field. Plotted in Figure (3.1) is an overview of simulation data; namely, we plot Nu, Re, and N as a function of Ra.

Throughout this chapter we present horizontal and vertical cross sectional views of the fluctuating temperature as visual representations of the flow field. The fluctuating temperature is a measure of the temperature with the mean (horizontally averaged) temperature neglected. In flow arrangements that are driven primarily by convection the fluctuating temperature is often a representative description of the flow morphology. For all flow visualizations listed using the fluctuating temperature, the colors red and blue denote positive and negative temperatures, respectively.

Q	Pr	Ra	Nu	Re	Δt	$N_x \times N_y \times N_z$	Cell Number	Steady	Box Size
1×10^2	1	7×10^2	1.01	0.84	1×10^{-3}	$192 \times 96 \times 96$	10	✓	10×10
1×10^2	1	1×10^3	1.53	1.55	1×10^{-3}	$192 \times 96 \times 96$	–	✘	10×10
1×10^2	1	5×10^3	2.67	5.97	1×10^{-3}	$192 \times 96 \times 96$	–	✘	10×10
1×10^2	1	1×10^4	3.30	8.34	5×10^{-5}	$192 \times 96 \times 96$	–	✘	10×10
1×10^2	1	2×10^4	4.05	11.42	5×10^{-5}	$288 \times 288 \times 96$	–	✘	10×10
1×10^2	1	4×10^4	5.06	16.09	5×10^{-5}	$288 \times 288 \times 96$	–	✘	10×10
1×10^2	1	1×10^5	5.69	24.68	5×10^{-5}	$384 \times 648 \times 96$	–	✘	10×10
1×10^2	1	1×10^6	13.07	100.14	5×10^{-6}	$384 \times 648 \times 96$	–	✘	7×7
1×10^4	1	7×10^2	1.12	0.56	5×10^{-5}	$192 \times 96 \times 96$	10	✓	10×10
1×10^4	1	1×10^3	1.71	1.55	5×10^{-5}	$192 \times 96 \times 96$	11	✓	10×10
1×10^4	1	5×10^3	3.64	7.17	5×10^{-5}	$192 \times 96 \times 96$	7	✓	10×10
1×10^4	1	1×10^4	4.69	11.80	5×10^{-5}	$48 \times 280 \times 96$	7	✓	10×10
1×10^4	1	2×10^4	6.04	19.15	5×10^{-5}	$48 \times 280 \times 96$	10	✓	10×10
1×10^4	1	4×10^4	8.46	29.37	5×10^{-5}	$192 \times 288 \times 96$	10	✓	10×10
1×10^4	1	6×10^4	8.89	40.35	5×10^{-5}	$98 \times 390 \times 96$	5	✓	10×10
1×10^4	1	2×10^5	9.01	81.55	2×10^{-5}	$384 \times 384 \times 140$	3	✓	10×10
1×10^4	1	4×10^5	8.05	87.33	5×10^{-5}	$384 \times 384 \times 140$	2	✓	10×10
1×10^4	1	6×10^5	8.33	100.30	5×10^{-7}	$96 \times 384 \times 96$	2	✓	10×10
1×10^4	1	2×10^6	12.38	251.67	5×10^{-6}	$192 \times 768 \times 120$	2	✘	6×6
1×10^4	1	1×10^7	19.44	649.46	5×10^{-6}	$576 \times 864 \times 120$	–	✘	4×4
1×10^6	1	1×10^4	4.70	11.82	5×10^{-6}	$48 \times 280 \times 96$	7	✓	10×10
1×10^6	1	2×10^4	6.05	19.15	5×10^{-6}	$48 \times 280 \times 96$	7	✓	10×10
1×10^6	1	4×10^4	7.75	30.75	5×10^{-6}	$48 \times 280 \times 96$	7	✓	10×10
1×10^6	1	6×10^4	8.95	40.47	5×10^{-6}	$48 \times 280 \times 96$	7	✓	10×10
1×10^6	1	2×10^5	13.55	90.46	5×10^{-6}	$48 \times 768 \times 96$	7	✓	10×10
1×10^6	1	6×10^5	21.13	241.95	5×10^{-6}	$96 \times 768 \times 140$	7	✓	7×7
1×10^6	1	2×10^6	18.00	919.73	5×10^{-7}	$96 \times 768 \times 140$	1	✓	4×4

Table 3.1: Details of numerical simulations. We specify the Chandrasekhar number (Q), the Prandtl number (Pr), the Nusselt number (Nu), the Reynolds number (Re), the time-step size (Δt), the spatial resolution ($N_x \times N_y \times N_z$), the number of convection rolls (Cell Number), whether the flow consists of steady rolls (✓) or otherwise (✘), and the box size. The critical Rayleigh number and critical horizontal wavenumber are $\mathrm{Ra}_c \approx 658$ and $k_c \approx 2.2215$, respectively. The box size is specified in units of the critical horizontal wavelength λ_c. We set k_c as the horizontal wavenumber for all the simulations listed.

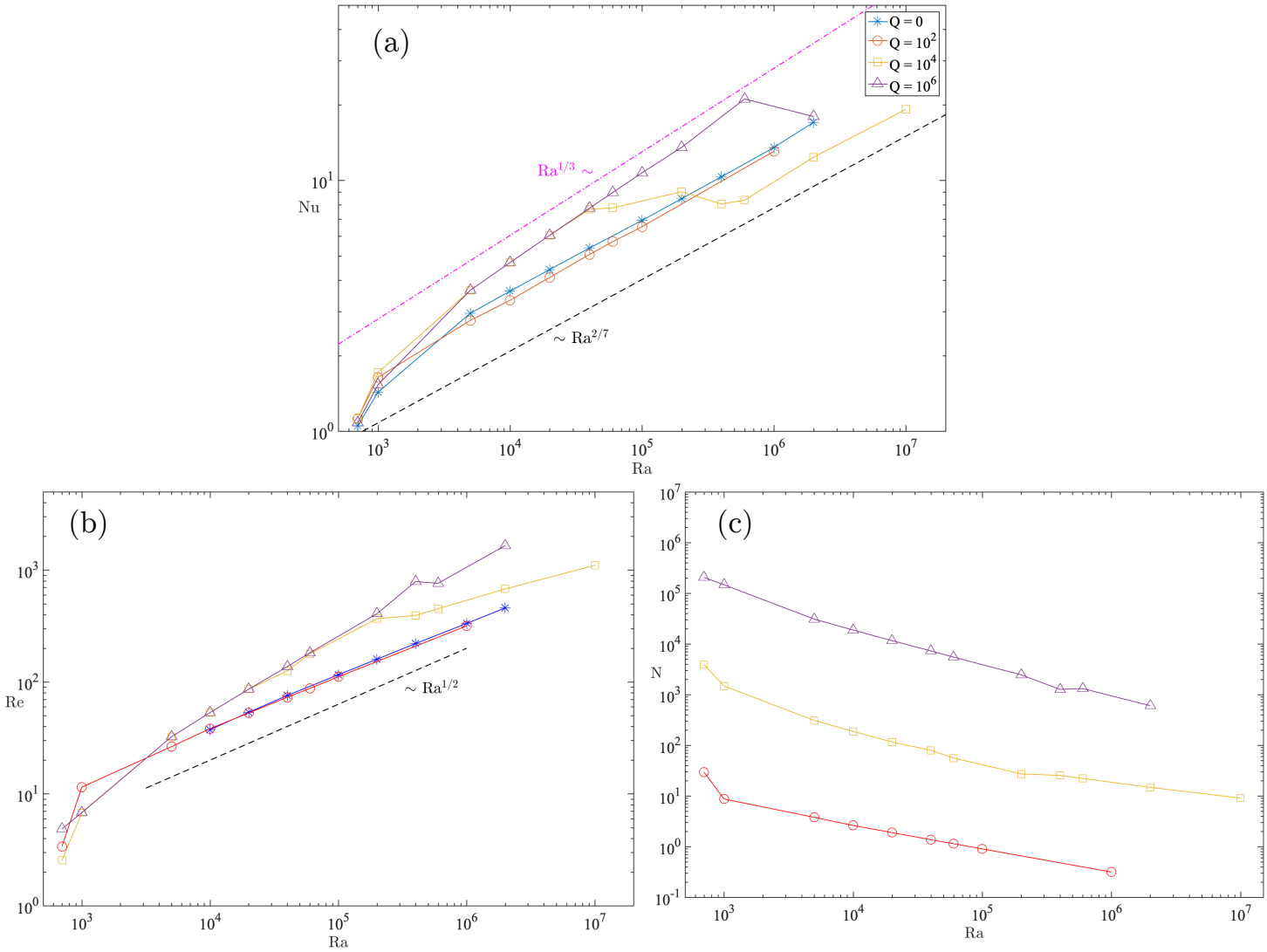

Figure 3.1: Output from the numerical simulations: (a): Heat transfer data as characterized by the Nusselt number (Nu) versus the Rayleigh number. (b): Reynolds number (Re) versus the Rayleigh number. (c): Interaction parameter (N) versus the Rayleigh number. We plot the results of varying magnetic field strengths as characterized by the Chandrasekhar number (Q). Power laws of $\mathrm{Nu} \sim \mathrm{Ra}^{1/3}$, $\mathrm{Nu} \sim \mathrm{Ra}^{2/7}$, and $\mathrm{Re} \sim \mathrm{Ra}^{1/2}$ are shown for reference.

3.1 The Weak Magnetic Field Regime

The weak magnetic field regime is primarily characterized by its inability to maintain a symmetric convective roll pattern along the direction of the magnetic field for Ra values larger than 700. As shown in the horizontal cross sectional view of the mid-plane in Figure (3.2), the convective roll pattern is ruptured by large scale modulations in the horizontal plane. Although the deviation from a strictly two-dimensional flow morphology is expected in the turbulent regime, and, indeed, is also found in the intermediate magnetic field regime, what makes $Q = 10^2$ unique is how rapidly the flow loses its two-dimensionality at relatively low values of Ra.

For Ra values on the order of 10^3 and larger we extrapolate a power law relating Nu to Ra. The so-called "free fall" similarity theory of $Nu \sim Ra^{1/3}$ was proposed by Priestly in 1954 [15] who derives the 1/3 power law in the limit of $Ra \to \infty$ by fixing the plate temperatures and allowing the separation distance to grow indefinitely. A well known phenomenological explanation of the approximate scaling $Nu \sim Ra^{2/7}$ was proposed by Castaing et. al in 1988 [4] in accordance with experimental evidence of turbulent convection flow. We calculate the power law relation to be

$$Nu \sim Ra^{0.29} \tag{3.4}$$

for Ra values between 10^3 and 10^6. Our data is in agreement with the 2/7 power law proposed previously.

3.1.1 Three-Dimensional Flow Structure

In the dynamical regime of $Ra \sim 10^4$ and larger we find a notable deviation from the convective roll pattern that had been previously shown to be the most unstable flow pattern. We demonstrate this new flow structure by discussing the case of $Ra = 6 \times 10^4$ as it is sufficiently larger than the critical Rayleigh number thereby serving as an appropriate representative of the more turbulent flow regime for Ra values between 10^4 and 10^6.

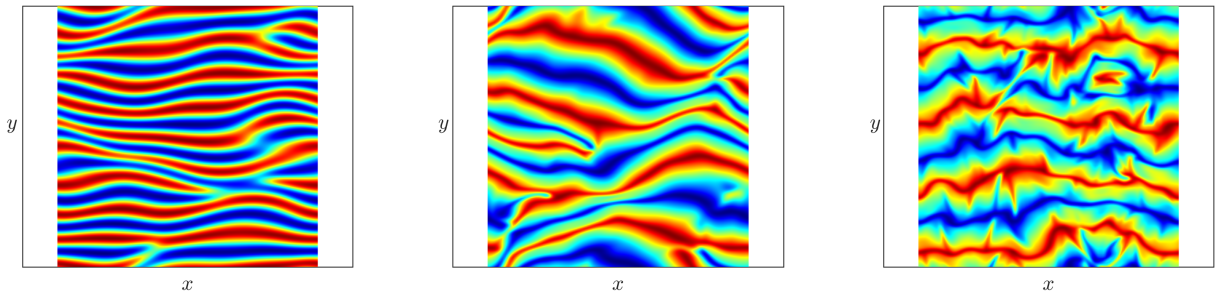

(a) Ra = 10^3 (b) Ra = 5×10^3 (c) Ra = 10^4

Figure 3.2: Horizontal cross sections of the fluctuating temperature are shown at the mid-plane for Q = 10^2; Ra = 10^3, 5×10^3, and 10^4.

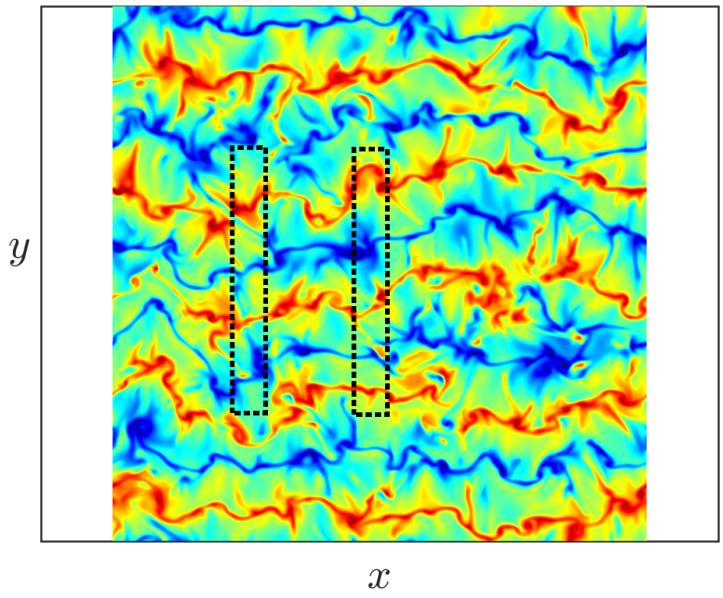

Figure 3.3: Horizontal cross section of the fluctuating temperature for the case of Q = 10^2, Ra = 6×10^4. The dashed lines represent the position of the vertical cross sections shown in Figure (3.4). Figure (3.4a) refers to the rightmost dashed region and and Figure (3.4b) refers to the leftmost dashed region.

A horizontal cross section of the fluctuating temperature for the specific case of Ra = 6×10^4 is shown in Figure (3.3). Despite the visible development of small-scale structures, the flow is primarily

anisotropic since there persists a preferential alignment along the direction of the magnetic field. Incidentally, the symmetric flow structure along the x-axis is broken. This asymmetric flow field is showcased in Figure (3.4) where we present vertical slices of the fluctuating temperature at varying positions parallel to the magnetic field lines. Figures (3.3) and (3.4) demonstrate that the weak magnetic field is capable of retaining an anisotropic flow structure but is incapable of maintaining a two-dimensional flow morphology.

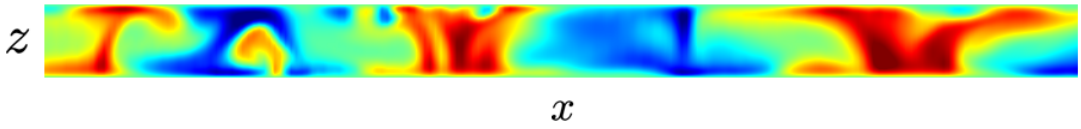

(a)

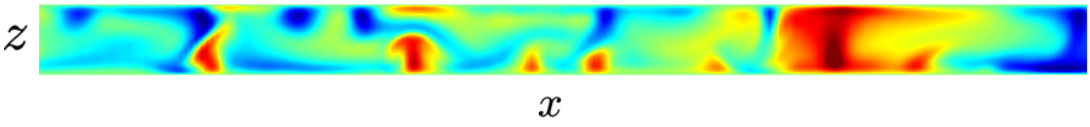

(b)

Figure 3.4: Vertical cross sections of the fluctuating temperature are shown at varying positions along the direction along the magnetic field. Here, Q = 10^2 and Ra = 6×10^4. Figure (3.4a) refers to the rightmost dashed region in Figure (3.3) and Figure (3.4b) refers to the leftmost dashed region in Figure (3.3). The flow is not symmetric along the direction of the magnetic field.

We further quantify the flow field's three-dimensionality by investigating the ratio of the kinetic energy along the direction of the magnetic field with the total kinetic energy, which we plot as a function of Ra in Figure (3.5). For Ra = 10^3 we note that the flow momentum is almost entirely contained in the vertical plane. As Ra increases we find that the kinetic energy along the direction of the magnetic field monotonically increases indicating that the flow morphology is becoming more three-dimensional. Our simulations further indicate an asymptotic relation between $\mathrm{KE}_x/\mathrm{KE}$ and Ra: namely, that the kinetic energy along the direction of the magnetic field shares 1/3 of the

flow field's total kinetic energy in the limit of large Ra. Indeed, as the visualizations of the flow further suggest, as Ra increases we find that the constraint of the magnetic field loses its dynamical relevance. Figure (3.6), a horizontal cross section of the fluctuating temperature for the case of Ra $= 10^6$, is a visual testament of how less anisotropic, and therefore more three-dimensional, the flow field is becoming.

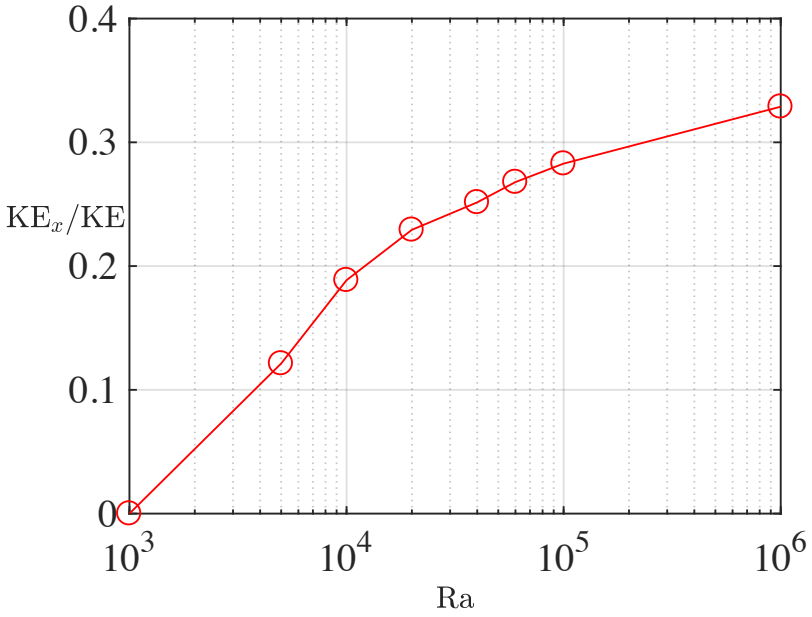

Figure 3.5: Ratio of the kinetic energy along the direction of the magnetic field to the total kinetic energy for the weak magnetic field (Q $= 10^2$).

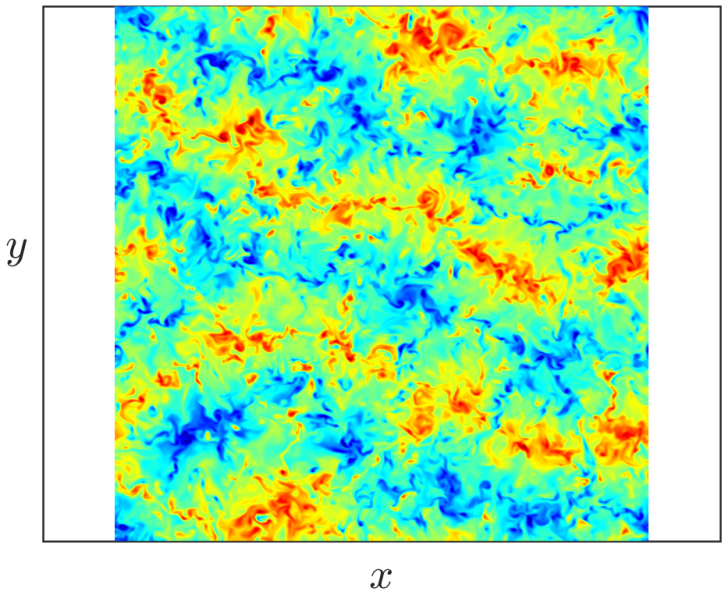

Figure 3.6: Horizontal cross section of the fluctuating temperature for Q = 10^2, Ra = 10^6. The flow appears to become more isotropic and three-dimensional as Ra increases.

Our proposed argument concerning the negligibility of the magnetic field in the increasing Ra regime may be supported by an inspection of the interaction parameter (N) as a function of Ra, as displayed in Figure (3.1c). A negative correlation between the interaction parameter and Ra can be observed, thereby suggesting that the magnetic field's effects on the dynamics depreciates as the flow field becomes more three-dimensional. A mathematical argument for this depreciation is proposed by noting that N is proportional to the inverse of Re since Q is independent of Ra. Figure (3.1b) further demonstrates a positive correlation between Re and Ra and thus the negative correlation between N and Ra is to be expected.

3.1.2 Thermal Boundary Layers

We observe the existence of thermal boundary layers in the weak magnetic field regime. A horizontally and temporally averaged vertical profile of the RMS perturbed temperature (i.e the temperature with the mean profile neglected) is displayed for Ra values of 10^4, 2×10^4, and 4×10^4

in Figure (3.7a). Noted in the vertical profile is the existence of thermal boundary layers which seem to widen as a function of Ra. The stretching thermal boundary layers is also seen in the vertical profile of the mean temperature plotted in Figure (3.7b). The existence of boundary layers permits conductive heat transfer to occur in small, isolated subspaces of the vertical domain. Convective heat transport occurs at and around the mid-plane where the fluid is allowed to mix.

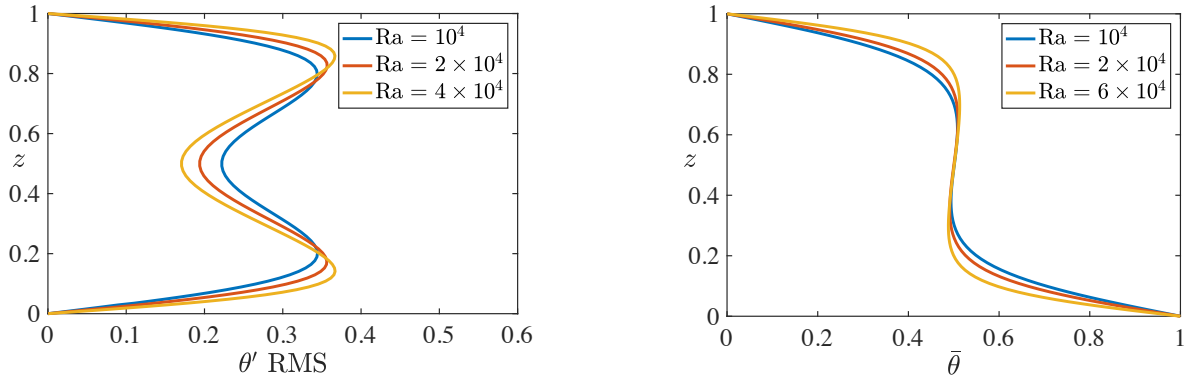

(a) (b)

Figure 3.7: Thermal profile data in the weak magnetic field regime (Q = 10^2): (a) RMS of the perturbed temperature (equal to the temperature of the fluid minus with the mean profile) for Ra = $10^4, 2\times10^4$ and 4×10^4. (b) Mean temperature profile for Ra = $10^4, 2\times10^4$, and 6×10^4. Thermal boundary layers, where the primary means of heat transport is conduction, is observed. A widening of the boundary layer is observed as Ra increases.

Thermal boundary layers have been observed in the literature. For example, numerical simulations of Rayleigh-Bénard convection conducted by T Hartlep, A Tilgner, and FH Busse [9] as well as experimental investigations by AE Perry and PH Hoffmann [13] all observe the existence of thermal boundary layers in turbulent flow regimes. Moreover, these thermal boundary layers are also investigated in numerical simulations of magnetoconvection by Xing-Xing Yu, Jie Zhang, and Ming-Jiu Ni [19]. With the existence of a boundary layer we note that a new dynamical length scale has been introduced — namely, the height of the boundary layer itself, traditionally labeled

δ. As such, we believe that future calculations involving δ may be utilized in order to further our understanding of the dynamics near the boundary.

3.1.3 Ohmic Dissipation in the Weak Magnetic Field Regime

For Ra values that are sufficiently large (namely, $\text{Ra} \geq 5\times10^3$) we observe that convective heat transport is reduced when compared to non-magnetic Rayleigh-Bénard convection. We hypothesize that this reduction in heat transport is due to ohmic dissipation. The dynamical significance of ohmic dissipation has been studied extensively. A. Tilgner [17] provides a general discussion of magnetic energy dissipation through a numerical study of rotating dynamos. A general expression for ohmic dissipation, ϵ_B, may be derived:

$$\epsilon_B = \frac{\text{Q}}{V}\int \left\langle (\nabla \times \mathbf{b})^2 \right\rangle dV = \frac{\text{Q}}{V}\int \left\langle \mathbf{j}^2 \right\rangle dV. \tag{3.5}$$

The two-dimensional roll structure, as we will demonstrate with the intermediate magnetic field regime, disallows the formation of an induced magnetic field. As such, we find that the two-dimensional magnetically constrained regime exhibits negligible ohmic dissipation. The weak magnetic field is incapable of maintaining the convective roll structure and thus we observe a non-vanishing current density.

Figure (3.8) supports the claim that there exists a positive correlation between Ra and the magnitude of the current density in the weak magnetic field regime. This positive correlation translates into an increase in the total amount of ohmic dissipation exhibited by the flow field. We find that the induced magnetic field acts like a source of drag for the system which tends to decrease convective heat transport. An exact, quantitative measure of ohmic dissipation as a function of Ra will be investigated in future studies. For the purposes of this thesis we solely propose that the existence of ohmic dissipation is evident and serves as a potential explanation for the reduction of Nu when compared to non-magnetic Rayleigh-Bénard convection. We discuss this point further in Section (3.2.1).

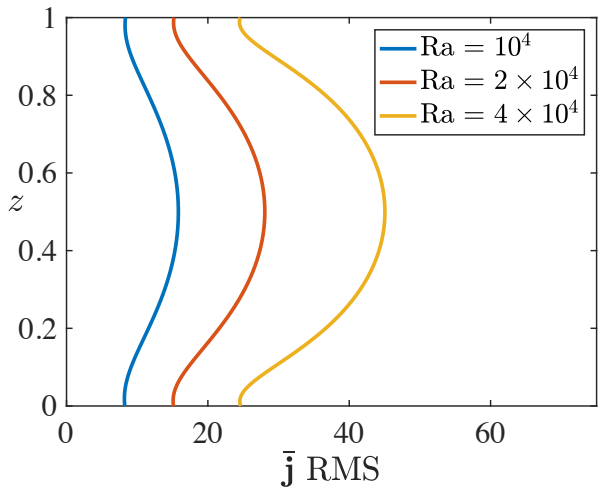

Figure 3.8: RMS of the horizontally and temporally averaged current density is plotted for Ra values of 10^4, 2×10^4, and 4×10^4 with Q = 10^2. The current density is observed to increase with Ra thereby suggesting an increase in total ohmic dissipation.

3.2 The Intermediate Magnetic Field Regime

The intermediate magnetic field regime, characterized by Q = 10^4, introduces dynamical regimes which differ substantially from the regimes discussed in the previous section with the weak magnetic field. Fixing Ra, we note that, as observed in Figure (3.1c), the interaction parameter in the intermediate magnetic field regime is two orders of magnitude larger than the interaction parameter of the weak magnetic field. Such a disparity in the magnitude of the interaction parameter suggests that the magnetic field will play a significant role in the dynamics of the system.

We attempt to extrapolate a power law relating Nu to Ra in the intermediate magnetic field regime. It may be observed from Figure (3.1a) that Nu scales with Ra differently depending on the magnitude of Ra. As such, we attempt to extrapolate different power laws for different ranges of Ra. Behaviorally, our results exhibit a power law for Ra values between 10^3 and 4×10^4 which exceeds the Nu $\sim$ $\mathrm{Ra}^{1/3}$ scaling law proposed by Priestly. Furthermore, restricting Ra strictly between 6×10^5 and 10^7 we find that the 2/7 power law is more appropriate. Our calculations support these

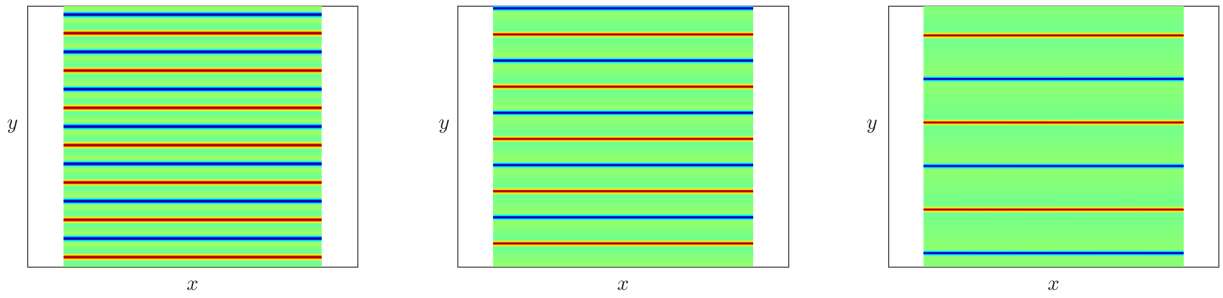

(a) $\mathrm{Ra} = 4 \times 10^4$ (b) $\mathrm{Ra} = 6 \times 10^4$ (c) $\mathrm{Ra} = 2 \times 10^5$

Figure 3.9: Horizontal cross sections of the fluctuating temperature are shown at the mid-plane for $\mathrm{Q} = 10^4$, $\mathrm{Ra} = 4 \times 10^4, 6 \times 10^4$, and 2×10^5. The flow consists of steady convection rolls despite Ra being on the order fo 10^4 and 10^5. As Ra increases there is a notable reduction in the number of convection cells sustained. The box size is constant in all 3 flow fields shown.

claims:

$$\begin{cases} \mathrm{Nu} \sim \mathrm{Ra}^{0.37} & \text{for} \quad \mathrm{Ra} \in [10^3, 4 \times 10^4] \\ \mathrm{Nu} \sim \mathrm{Ra}^{0.28} & \text{for} \quad \mathrm{Ra} \in [6 \times 10^5, 10^7] \end{cases} \tag{3.6}$$

3.2.1 Two-dimensional Flow Structure

We first discuss the intermediate magnetic field's ability to mediate a stable convective roll pattern. Indeed, as the horizontal cross sections of the flow field in Figure (3.9) indicate, two-dimensional convection rolls are maintained by the intermediate magnetic field despite Ra being on the order of 10^5. Figure (3.10) contrasts the flow field under the influence of the intermediate magnetic field with the flow field of non-magnetic Raleigh-Bénard convection through horizontal and vertical cross sections of the fluctuating temperature.

As suggested by Figure (3.10a), the absence of the intermediate magnetic field permits the existence of chaotic, turbulent flow regimes that may be characterized as unstructured. The unstructured nature of this chaotic dynamical regime is particularly showcased in Figure (3.10b) as no obvious flow pattern may be determined. This is contrasted with the smooth, ordered roll structure that is achieved through the stabilizing force of the intermediate magnetic field. Moreover, Figure (3.10c) suggests that the intermediate magnetic field supports large-scale two-dimensional roll

structures which efficiently mediate convective heat transfer when compared to the regime with no magnetic field.

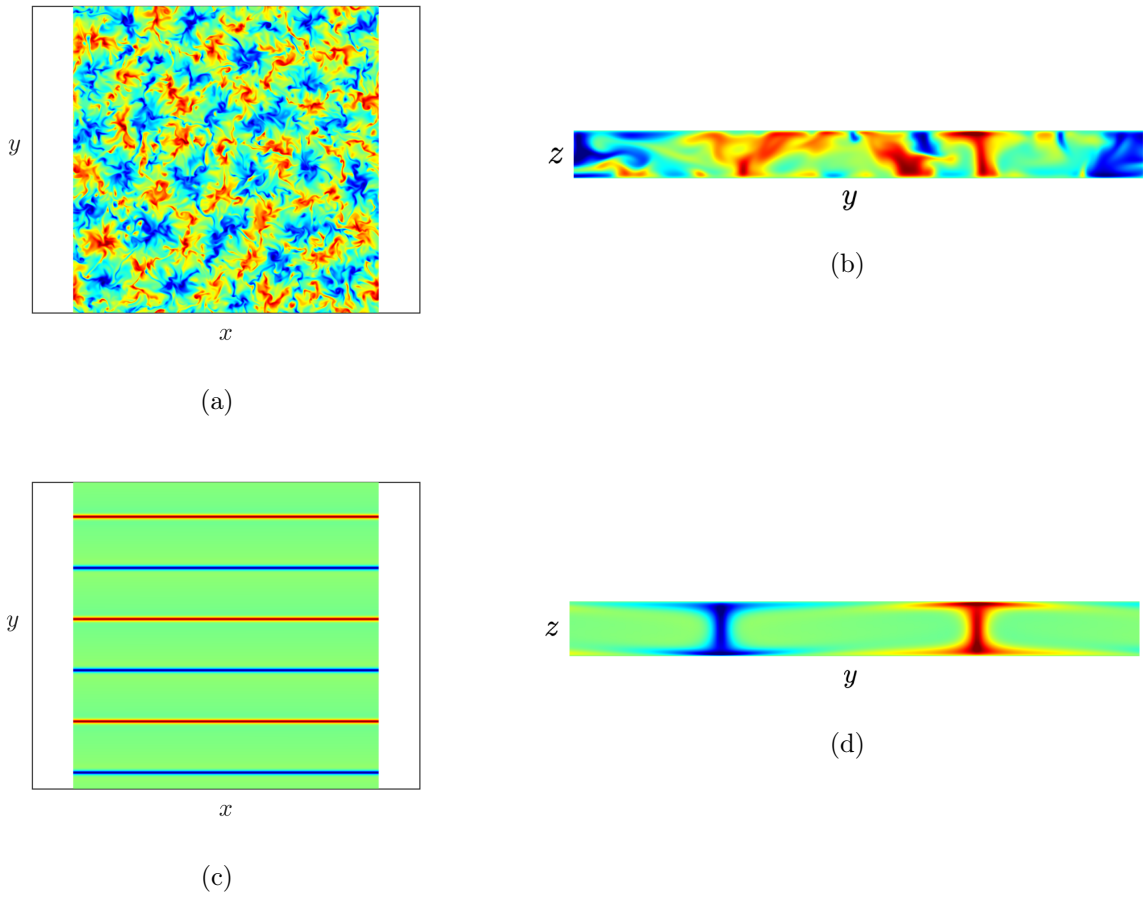

Figure 3.10: Horizontal and vertical cross sections of the fluctuating temperature is contrasted between Q = 0, Ra = 10^5 (Figures (3.10a) and (3.10b) represent the horizontal and vertical cross sections, respectively) and Q = 10^4, Ra = 2×10^5 (Figures (3.10a) and (3.10b) represent the horizontal and vertical cross sections, respectively).

It is evident from Figure (3.1a) that the intermediate magnetic field permits a dynamical regime with more efficient heat transfer when compared to regular Rayleigh-Bénard convection. Fixing Ra while simultaneously restricting our considerations to Ra values between 10^3 and 4×10^4, we notice that convective heat transfer is enhanced with the addition of the intermediate magnetic

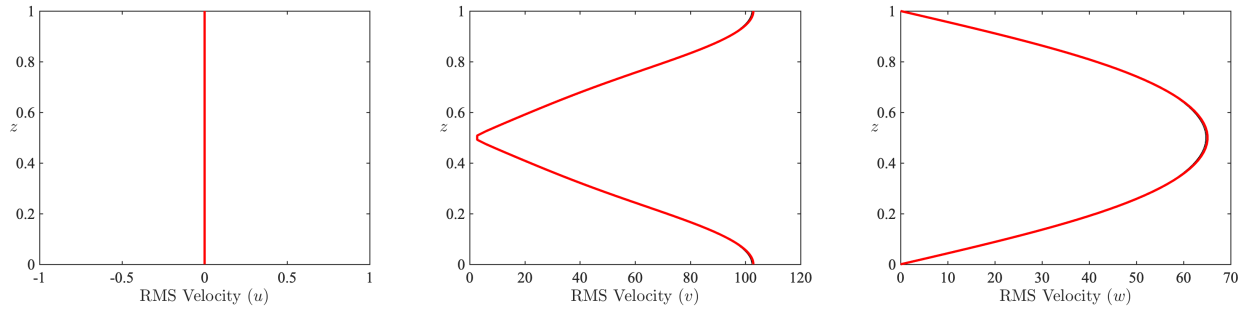

(a) (b) (c)

Figure 3.11: Horizontal and temporal average of the RMS flow velocity is shown as a function of height for Q = 10^4 and Ra = 2×10^4.

field. This notable increase in convective efficiency may be attributed to multiple factors which we now discuss.

We plot the horizontally and temporally averaged RMS flow velocity in Figure (3.11) for the case of Ra = 2×10^4 which serves as a representative of the two-dimensional flow regime. The flow along the vertical plane is circular, thereby signifying the existence of convection rolls. We further find that the flow velocity along the direction of the magnetic field is negligible when compared to the flow along the vertical plane. As we argued with the weak magnetic field flow regime, a minimal transfer of momentum along the horizontal plane is ideal for convection since it maximizes heat transfer between the two boundary plates.

3.2.2 Anisotropic Turbulence

In the intermediate magnetic field regime, we note that the case characterized by Ra = 6×10^4 represents the first instance in which a deviation from the 0.37 power law can be observed. As suggested by Figure (3.9), the flow structure in the case of Ra = 6×10^4 is primarily two-dimensional. Moreover we note that Figure (3.9) showcases a negative correlation between the number of convective cells and the efficiency of heat transfer. It is important to note that the interaction parameter for the case of Ra = 6×10^4 is comparable in magnitude to the interaction parameters in the regime of the weak magnetic field. This result suggests that a relationship may

exist between the interaction parameter and the efficiency of convective heat transfer. Future studies involving varying magnetic field strengths may be able to confirm our hypothesis.

Increasing Ra further, a deviation from the two-dimensional rolling flow field starts to develop and we observe a novel dynamical regime which is not observed under the influence of the weak magnetic field. In particular, Figure (3.12) suggests the existence of a transitionary phase between two-dimensional roll structures and three-dimensional isotropic turbulence. It was hypothesized that we would observe strictly two-dimensional turbulence (namely, small scale structures developing in the vertical plane but not along the direction of the magnetic field) but this behavior is not observed. Instead, we observe a transitional phase which we label "anisotropic turbulence."

The anisotropic turbulence transitional phase is primarily characterized by the coexistence of small scale structures and a preferred flow alignment along the the direction of the magnetic field. The flow behavior in Figure (3.12) showcases convectional roll structures which, coupled with an increasing Ra, are deformed by large-scale modulations along the direction of the magnetic field. We characterize the flow field along the horizontal plane as primarily structured: the deviations from the convective roll pattern shown in Figures (3.12a), (3.12c), and (3.12e) are small and do not significantly disrupt the preferred alignment of the flow. The two-dimensional vertical plane, as shown in Figures (3.12b), (3.12d), and (3.12f), is significantly altered by an increase in Ra. A notable spread of the rolling flow field is visible for $\mathrm{Ra} \sim 10^5$. At $\mathrm{Ra} = 2 \times 10^6$ we observe a significant deviation from the convective cell pattern that was previously stabilized by the intermediate magnetic field. We therefore characterize the anisotropic turbulence transitional phase by the intermediate magnetic field's simultaneous ability of maintaining a preferred flow alignment along the direction of the magnetic field while also permitting small-scale structures to form in the vertical and horizontal planes, thereby deviating away from the two-dimensional convective roll pattern which was present for lower values of Ra.

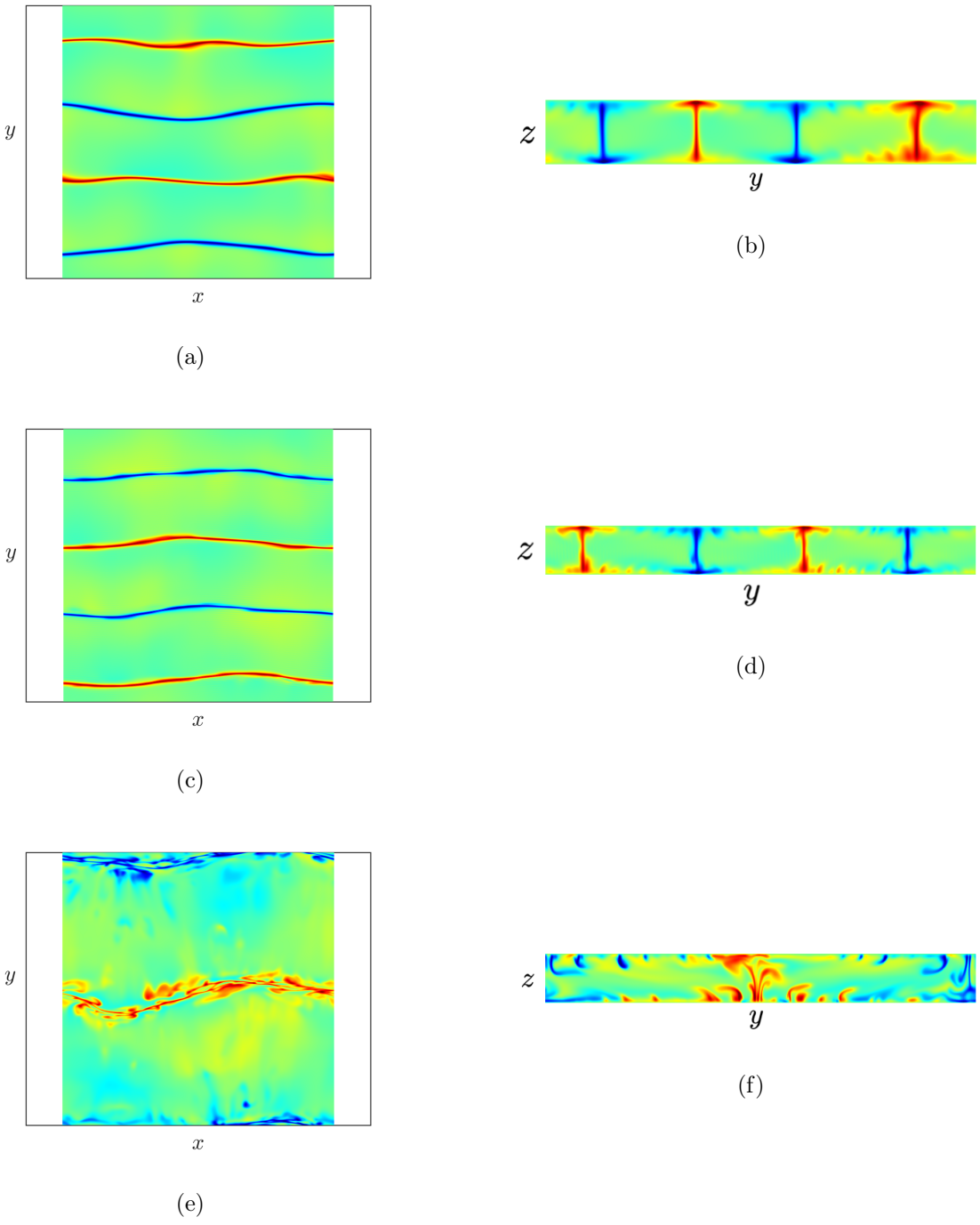

Figure 3.12: Horizontal and vertical cross sectional views of the fluctuating temperature is presented for various Ra values under the influence of the intermediate magnetic field (Q = 10^4). From top to bottom: Ra = 4×10^5, 6×10^5, and 2×10^6.

3.2.3 Ohmic Dissipation and Steady Time Evolutions

We return to the discussion on ohmic dissipation. As argued previously, the convective roll structure present in the stable dynamical regime suppress the formation of an induced magnetic field. Indeed, we observe a vanishing current density in the intermediate magnetic field regime. The lack of an induced magnetic field in this flow regime is explained by the induction equation. A two-dimensional roll structure prohibits any variation in the flow velocity along the direction of the imposed magnetic field. As such, equation (2.13) forces $\mathbf{b}$ to equal zero.

Within the weak magnetic field regime we observed that the induced magnetic field acted as a source of drag for the system. The two-dimensional flow field is free from such drag. Moreover, the non-existence of an induced magnetic field necessarily implies that there is no source of ohmic dissipation in the system. We propose that the lack of ohmic dissipation may contribute to the increased efficiency in convective heat transfer that is exhibited by the convective roll regime.

We note that the two-dimensional regime is further characterized by having a steady Nu time series, as portrayed in Figure (3.13). With our numerical simulations there always exists an initial transient period in which the flow behavior is extremely erratic. This initialization period is disregarded in all calculations and visualizations since it is does not directly refer to any physical phenomena. It is visible from Figure (3.13a) that the weak magnetic field presents a Nu time series which contains numerous small-scale oscillations. The intermediate magnetic field case in Figure (3.13b) presents a steady time evolution since the small-scale oscillations are not present. Moreover, the statistical quantities obtained from the intermediate magnetic field cases are much less computationally demanding since the flow pattern is essentially fixed in time. The weak magnetic field cases, on the other hand, must be observed over an extensive period of time in order to obtain statistically reliable time averages.

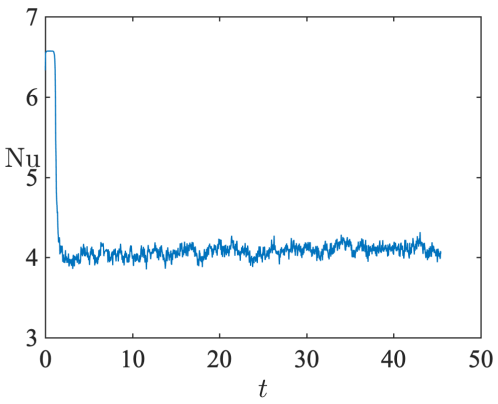

(a)
$Q = 10^2$

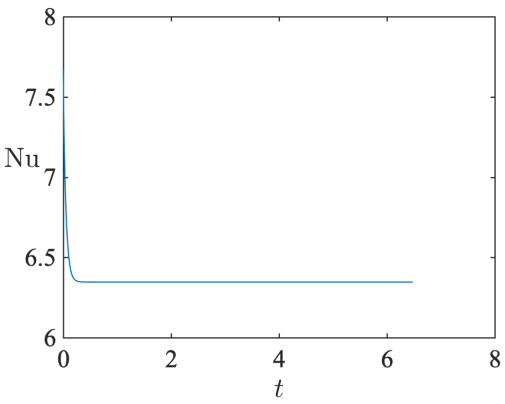

(b)
$Q = 10^4$

Figure 3.13: Nusselt number (Nu) time series for $Q = 10^2$ compared with $Q = 10^4$ for Ra fixed at 2×10^4. The intermediate magnetic field regime maintains a steady time series. The Nu time series for the weak magnetic field exhibits small oscillations.

3.3 The Strong Magnetic Field Regime

The strong magnetic field regime is defined by $Q = 10^6$. The interaction parameter for the strong magnetic field is orders of magnitude larger than the intermediate magnetic field. We previously found that the intermediate magnetic field was sufficiently strong enough to magnetically constrain the flow morphology into being two dimensional for a large range of Ra values. The strong magnetic field behaves similarly: for Ra values between 10^3 and 6×10^5 we notice a 0.37 power law relating Nu to Ra from Figure (3.1a). Our calculations yield the following scaling relation between Nu and Ra:

$$\mathrm{Nu} \sim \mathrm{Ra}^{0.37} \tag{3.7}$$

for the restricted domain of $\mathrm{Ra} \in [10^3, 6 \times 10^5]$. The two-dimensional roll structure of this regime suggests that the 0.37 power law may apply to flow fields which primarily consist of convective rolls.

Moreover, Figure (3.1a) seems to suggest that there exists an asymptotic relationship between Nu and Q. Although Nu is generally enhanced when we compare cases from the weak and intermediate magnetic field regimes at a fixed Ra, we note that, at least in the two-dimensional flow regime,

there is no observable increase in convective effeciency upon transitioning from the intermediate to the strong magnetic field regime. This result seems to suggest a horizontally imposed magnetic field benefits heat transfer only in its ability to maintain a two-dimensional flow; once the convective roll structure has been achieved it appears as if increasing the magnetic field strength contributes nothing to the efficiency of convective heat transfer.

The case of $\mathrm{Ra} = 2 \times 10^6$ is the first case to deviate away from the 0.37 power law respected by the vast majority of cases in the strong magnetic field regime ($10^3 \leq \mathrm{Ra} \leq 6 \times 10^5$). We observe from Figure (3.1c) that this deviation occurs when the interaction parameter is comparable in magnitude to the interaction parameter of $\mathrm{Ra} \sim 10^4$ for the intermediate magnetic field cases. Moreover, the first deviation from the 0.37 power law for the intermediate magnetic field regime occurs when $\mathrm{Ra} \sim 10^4$. This comparability in N further supports our previous observation that the interaction parameter plays an important role in differentiating between the dynamical regimes of differing convective efficiency.

We investigate the case of $\mathrm{Ra} = 2 \times 10^6$ in more detail. A visualization of the fluctuating temperature is shown in Figure (3.14) for the cases of $\mathrm{Ra} = 6 \times 10^5$ and 2×10^6. The flow velocity along the direction of the magnetic field is negligible compared to the flow velocity contained in the vertical plane, this is demonstrated by the two-dimensional flow morphology. As argued previously, since the flow is predominately two-dimensional, we cannot attribute the reduction in Nu to ohmic dissipation due to the negligibility of the induced magnetic field. Instead, we propose that drop in convection cell number is responsible for the reduction in Nu.

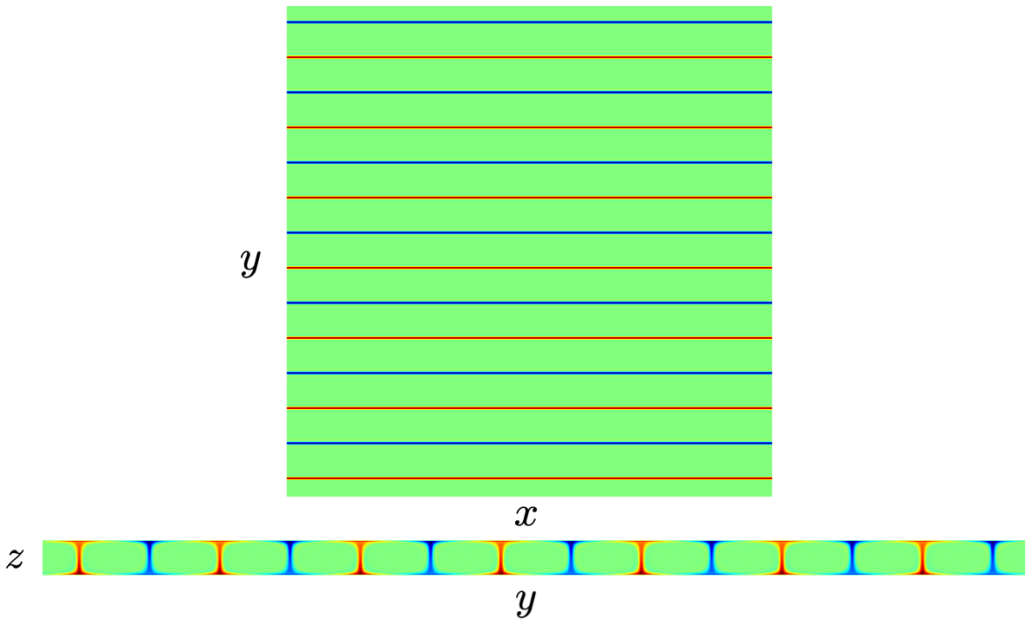

(a)

$\mathrm{Ra} = 6 \times 10^5$

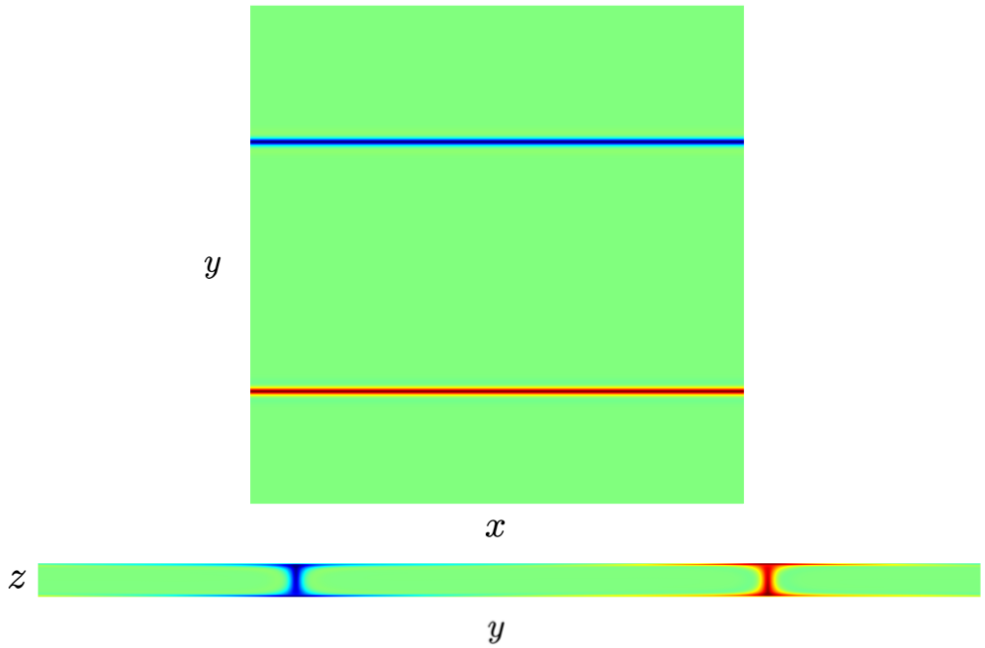

(b)

$\mathrm{Ra} = 2 \times 10^6$

Figure 3.14: Horizontal and vertical cross section of the fluctuating temperature for the case of Q $= 10^6$, Ra $= 2 \times 10^6$. A notable drop in convective cell number is observed, potentially explaining the deviation from the Nu $\sim$ Ra$^{2/7}$ power law. The box size is not constant between these two cases yet we suggest that the reduction in Nu is still physical.

We note that the increase in Ra from 6×10^5 to 2×10^6 appears to have dropped the cell number significantly: from 7 to 1. Part of the reason why this drop in cell number is so drastic is because, as Table (3.1) demonstrates, there has been a reduction in the total box size between these two cases. The change of box size was intended to circumvent the need to increase the spatial resolution of our simulation, since shrinking the box size is more computationally efficient than increasing the spatial resolution. We believe that the reduction in Nu depicted by this simulation is still physical and not just an artificial byproduct of the change in box size. Our justification for this assertion is as follows. It was previously argued that the deviation from the 0.37 power law for the intermediate magnetic field case was primarily due to the reduction in total cell number. Indeed, the interaction parameter for when that decrease in cell number occured ($\mathrm{Ra} \sim 6 \times 10^4$) in the intermediate magnetic field case is comparable to the interaction parameter of the $\mathrm{Ra} = 2 \times 10^6$ case that is currently being discussed in the strong magnetic field regime. Given the apparent dynamical significance of the interaction parameter in the context of differentiating flow regimes, we hypothesize that the reduction in convective cell number is physical and not just due to the change in box size.

It should also be pointed out that reducing the box size may also increase the steadiness of the roll structure. Observationally, this may be motivated by noting how the convection cells in Figure (3.14a) for $\mathrm{Ra} = 6 \times 10^5$ are significantly thinner than the convection cells in Figure (3.14b) for $\mathrm{Ra} = 2 \times 10^6$. Given the disparity in flow steadiness and how, at a similar magnitude in interaction parameter, a similar deviation from the 0.37 power law was observed in the intermediate magnetic field regime, we hypothesize that the reduction in Nu in the strong magnetic field regime is a physical phenomenon.

Preliminary simulations were conducted to investigate the effects of a change in box size on the dynamics of the system but no rigorous results have been deduced. This was not a primary concern of our project since a variable box size is common in the literature. Numerical studies of two-dimensional Rayleigh-Bénard convection conducted by Johnston and Doering [10] suggest that a change in "box size" (in their case it is an aspect ratio since their simulations are two-dimensional)

does not significantly alter the relationship between Nu and Ra. We recognize that the effects of a variable box size may inadvertently affect the efficiency of convective heat transfer. The topic of varying box sizes will be investigated in future studies.

Chapter 4

Conclusion

The wide range of Ra values investigated coupled with the varying magnetic field strengths introduced interesting dynamical regimes. We demonstrated that the weak magnetic field ($Q = 10^2$) was strong enough to maintain a preferred flow alignment but was generally incapable of maintaining the two-dimensional roll structure. The fraction of kinetic energy along the direction of the magnetic field generally increased with Ra thereby showcasing an inclination for the flow to become more three-dimensional. We further proposed that the reduction in Nu when compared to non-magnetic Rayleigh Bénard convection was attributed to the existence of a non-zero current density serving as a source of ohmic dissipation in the system. For the vast majority of the cases discussed in the weak magnetic field regime (namely, for Ra values between 10^3 and 10^6) our simulations demonstrated a $Nu \sim Ra^{2/7}$ scaling law.

The intermediate ($Q = 10^4$) and strong ($Q = 10^6$) magnetic field regimes maintained laminar, two-dimensional rolling flow structures for Ra values orders of magnitude larger than the critical Rayleigh number. We observed a 0.37 power law relating Nu to Ra when the convective rolls were present. In the steady, two-dimensional regime we note that Nu is enhanced when compared to non-magnetic Rayleigh-Bénard convection. This is primarily due to the convective roll's effective heat transport structure. Furthermore, for the same 2D convective roll regime, we observe no significant increase in efficiency in heat transport between the $Q = 10^4$ and $Q = 10^6$ cases while holding Ra fixed. Moreover, the two-dimensionality of the flow field suppressed ohmic dissipation in the system.

For $Q = 10^4$, a loss in cell number correlated with a deviation away from the 0.37 power

law. For Ra values between 6×10^5 and 10^7 we noticed that our cases followed a $\mathrm{Nu} \sim \mathrm{Ra}^{2/7}$ scaling law. In the same Ra regime we observed small scale turbulent flow structures as well as large scale-modulations along the direction of the magnetic field. Two-dimensional turbulence was not observed in any of the magnetic field regimes discussed.

In the strong magnetic field regime we noticed that the convective roll structure persisted in all of the cases investigated (up to $\mathrm{Ra} = 2 \times 10^6$). With $\mathrm{Ra} = 2 \times 10^6$ we observed a notable deviation away from the 0.37 power law relating Nu to Ra. Similar to the case when $\mathrm{Q} = 10^4$ we found that this reduction in Nu coincided with a significant drop in convective cell number. We hypothesized that a drop in cell number is correlated with a reduction in Nu. Although we observed anisotropic turbulence in the intermediate magnetic field regime no such regimes were observed under the influence of the strong magnetic field.

In terms of future studies, we notice significant correlations between the steadiness of the flow field and the interaction parameter. Investigations with imposed magnetic field strengths of varying magnitude could allow us to determine some critical values of the interaction parameter in which one would expect steady or unsteady flow patterns.

The subject of ohmic dissipation and its relation to the reduction in Nu is also a source of interesting investigation. With the weak magnetic field regime we noticed a negative correlation between ϵ_B and Nu. We aim to calculate ϵ_B for each of the cases we discussed in the hopes of concluding a more rigorous relationship between ohmic dissipation and the efficiency of convective heat transport.

Lastly, we noticed that a reduction in the efficiency of convection correlated with a drop in the total box size simulated. We hypothesized that the drop in Nu was physical and not just an artificial byproduct of the smaller box size. In recognition that that the effects of a smaller box may effect Nu's behavior in manners that we may not initially expect, we hope to simulate the effects of a change in box size on different flow regimes as a way of rigorously testing our assumptions.

Bibliography

[1] BS Bhadauria. Time-periodic heating of rayleigh–benard convection in a vertical magnetic field. Physica Scripta, 73(3):296, 2006.

[2] FH Busse. Non-linear properties of thermal convection. Reports on Progress in Physics, 41(12):1929, 1978.

[3] FH Busse and CR Carrigan. Laboratory simulation of thermal convection in rotating planets and stars. Science, 191(4222):81–83, 1976.

[4] Bernard Castaing, Gemunu Gunaratne, François Heslot, Leo Kadanoff, Albert Libchaber, Stefan Thomae, Xiao-Zhong Wu, Stéphane Zaleski, and Gianluigi Zanetti. Scaling of hard thermal turbulence in rayleigh-bénard convection. Journal of Fluid Mechanics, 204:1–30, 1989.

[5] Subrahmanyan Chandrasekhar. Hydrodynamic and hydromagnetic stability. Courier Corporation, 2013.

[6] Ulrich R Christensen and Julien Aubert. Scaling properties of convection-driven dynamos in rotating spherical shells and application to planetary magnetic fields. Geophysical Journal International, 166(1):97–114, 2006.

[7] Philip G Drazin. Introduction to hydrodynamic stability, volume 32. Cambridge university press, 2002.

[8] George E Hale, Ferdinand Ellerman, Seth Barnes Nicholson, and Alfred Harrison Joy. The magnetic polarity of sun-spots. The Astrophysical Journal, 49:153, 1919.

[9] T Hartlep, A Tilgner, and FH Busse. Transition to turbulent convection in a fluid layer heated from below at moderate aspect ratio. Journal of Fluid Mechanics, 544:309–322, 2005.

[10] Hans Johnston and Charles R Doering. Comparison of turbulent thermal convection between conditions of constant temperature and constant flux. Physical review letters, 102(6):064501, 2009.

[11] Pijush K Kundu and IM Cohen. Fluid mechanics. 2004. Google Scholar, pages 157–158, 2008.

[12] P Marti, MA Calkins, and K Julien. A computationally efficient spectral method for modeling core dynamics. Geochemistry, Geophysics, Geosystems, 17(8):3031–3053, 2016.

[13] AE Perry and PH Hoffmann. An experimental study of turbulent convective heat transfer from a flat plate. Journal of Fluid Mechanics, 77(2):355–368, 1976.

[14] Roger Peyret. Spectral Methods for Incompressible Viscous Flow. Springer, 2002.

[15] CHB Priestley. Convection from a large horizontal surface. Australian Journal of Physics, 7(1):176–201, 1954.

[16] Lord Rayleigh. Lix. on convection currents in a horizontal layer of fluid, when the higher temperature is on the under side. The London, Edinburgh, and Dublin Philosophical Magazine and Journal of Science, 32(192):529–546, 1916.

[17] A Tilgner. Magnetic energy dissipation and mean magnetic field generation in planar convection-driven dynamos. Physical Review E, 90(1):013004, 2014.

[18] David J Tritton. Physical fluid dynamics. Springer Science & Business Media, 2012.

[19] Xing-Xing Yu, Jie Zhang, and Ming-Jiu Ni. Numerical simulation of the rayleigh-benard convection under the influence of magnetic fields. International Journal of Heat and Mass Transfer, 120:1118–1131, 2018.